Subsurface Flow and Transport Through a Snowmelt-recharged Hillslope Constrained with Multiyear Water Balance

Tetsu K. Tokunaga[1], Jiamin Wan[1], Ahn Phuong Tran[2], Wenming Dong[1], Alexander W. Newman[3], Curtis A. Beutler[3], Wendy Brown[3], Amanda N. Henderson[3], and Kenneth H. Williams[1]

[1]Lawrence Berkeley National Laboratory, Berkeley, California, USA
[2]Water Research Institute, Hanoi, Vietnam
[3]Rocky Mountain Biological Laboratory, Crested Butte, Colorado, USA

Corresponding author: Tetsu K. Tokunaga (tktokunaga@lbl.gov)

Key Points:

- Large contrasts in annual precipitation are useful for constraining hydraulic conductivity profiles estimated by transmissivity feedback
- Exports during snowmelt occur primarily within shallow depths through highly transmissive saturated soils, except in snow drought years
- A framework is presented for estimating subsurface flow and transport on hillslopes based on sparsely distributed measurements

Abstract

Quantifying flow and transport from hillslopes is vital for understanding surface water quality, but remains obscure because of limited subsurface measurements. A recent combination of water mass balance over a single year with the transmissivity feedback model for a lower montane hillslope in the East River watershed (Colorado) left large uncertainties in transmissivities and predicted fluxes. Because snowmelt drives subsurface flow on this hillslope, improved constraints on the transmissivity profile were obtained by optimizing flux predictions over years having large differences in precipitation minus evapotranspiration. The optimized field-scale hydraulic properties combined with water table elevations predict groundwater discharges that are consistent with wide ranges of snowmelt. As snowmelt rapidly raises the water table, solutes released primarily through bedrock weathering are largely transported out of the hillslope via its highly transmissive soil. Such pulsed water and solute exports along the soil are minimized during snow drought years. Although solute concentrations generally are lower in soils relative to the underlying weathering zone, solute exports during high recharge occur predominantly via soil because of its enlarged transmissivities under snowmelt-saturated conditions. In contrast, this shallow pathway is negligible when recharge and water table elevations are low. The multiyear calibrated subsurface properties combined with updated pore water chemistry continue to show that the weathering zone is the primary source of base cations and reactive nitrogen released from the hillslope. Subsurface export predictions can now be obtained for wide ranges of snowmelt based on measurements of water table elevation and profiles of pore water chemistry.

1 Introduction

Understanding distributions of subsurface flow and transport in hillslopes is needed for predicting a number of important processes including exports into riparian zones and surface waters (Jencso et al., 2010; McGuire & McDonnell, 2010; Penna et al., 2015; Spencer et al., 2021), bedrock weathering (Ameli et al., 2017; Anderson & Dietrich, 2001; Wan et al., 2019), and slope stability (Arnone et al., 2011; Godt et al., 2008; Uchida et al., 2001). However, the heterogeneous subsurface hydraulic properties that modulate flow can only be sparsely characterized, and local measurements in soil and shallow saprolite are known to severely underestimated values of K needed to represent flow at the hillslope scale (Brooks et al., 2004; Di Prima et al., 2018; Glaser et al., 2019; Glaser et al., 2016; Uchida et al., 2001; Weiler et al., 2005; Wilson et al., 2016). Moreover, sampling of pore waters is similarly limited for capturing the spatially complex aqueous geochemistry of the hillslope subsurface (Boggs & Adams, 1992; Weihermuller et al., 2006). Thus, simplifying approximations are needed in order to predict hillslope behavior based on sparse local measurements. In hillslopes where profiles of the hydraulic conductivity K increase towards to the soil surface, the transmissivity feedback model (Bishop et al., 2004; Kendall et al., 1999; Rodhe, 1989) provides a practical simplification for the problem of groundwater flow responses to recharge events. The transmissivity feedback model describes downslope flow responses to rainfall or snowmelt recharge through accommodating new recharge within a rising water table, i.e., within a thicker and hence more transmissive saturated zone. However, transmissivity feedback alone leaves absolute magnitudes of total subsurface flow unconstrained.

We recently applied an estimate of total subsurface flow over the course of one year to help constrain transmissivity feedback calculations for a four layer hillslope system consisting of fractured bedrock, weathering zone, subsoil, and surface soil, and introduced an approach for

predicting subsurface concentration-discharge (*C*-*Q*) relations (T. K. Tokunaga et al., 2019). This methodology provided a framework for quantifying chemical weathering of bedrock (Wan et al., 2019), and for explaining the importance of bedrock weathering for nitrogen (N) exports to the hydrosphere and atmosphere (Wan et al., 2021). In those recent applications, the difference between cumulative precipitation *P* and calculated evapotranspiration *ET* for a single year (from 12-1-2016 to 11-30-2017) was equated with the net subsurface flow for that time interval, and transmissivities were adjusted within different layers in order to meet this water mass balance requirement. This mass balance constraint indicated that measured soil and weathering zone *K* values obtained from steady-state flow in auger holes were not high enough to accommodate the required subsurface discharge, consistent with conclusions from the previously cited studies. We also found that combinations of widely ranging *K* values were able to match the required net subsurface flow over the year, leaving high levels of uncertainty for flow and transport within each layer. Because the chemistry of pore waters varies among the different zones, the uncertainties in *K* largely dictate the uncertainties in overall solute exports from the hillslope, and point to the need for improving estimates of flow. The hillslope scale effective *K* values can be refined by optimizing predicted subsurface fluxes over years with large differences in both water table dynamics and *P*-*ET*, because these conditions encompass years with large contrasts in downslope flow along the highly permeable soil layer.

In the present work, the mass balanced transmissivity feedback approach is improved through calibrating the *K* profile for compatibility with wide ranges in annual *P*–*ET*, and through better representation of *P* and *ET* by using data from a weather station closer to the hillslope. The ability to accommodate large variations in annual recharge with transmissivity feedback discharge predictions is important in view of highly variable annual snowfall (Cayan, 1996; Lute & Abatzoglou, 2014; Woodhouse & Pederson, 2018; Xiao et al., 2018), and potential increased frequency of snow drought years under changing climate (Dierauer et al., 2019; Marshall et al., 2019; Shrestha et al., 2021). These considerations also improved estimates of the partitioning of downslope flow along the different zones throughout each water year. Changes to fluxes resulting from multiyear water balances and more representative weather data also alter predictions concerning subsurface solute exports. This warranted developing improved estimates of bedrock weathering and N export rates that are included here.

2 Methods

Details of the hillslope hydrologic characterization were presented previously (T. K. Tokunaga et al., 2019). Here, an overview of the hillslope site is provided, followed by updated descriptions of the annual water balance approach, hydraulic gradient monitoring, hydraulic properties calculations, and pore water quality measurements.

2.1. Site description

This meadows-vegetated hillslope in the Colorado Rocky Mountains (U.S.A.) is situated on a northeast facing slope, and drains into a willows-vegetated floodplain along the upper East River (Figure 1a). Topography is used to delineate surface boundaries of the hillslope system. From its local peak (2936 m elevation), the nearly 1 km long drainage transect consists of upper and lower hillslope segments that drain into a floodplain of the East River. The East River flows into the Gunnison River, a major tributary of the Colorado River. The upper hillslope segment is not monitored, but provides about 72% of the total subsurface flow exiting the lower transect based on its topography and horizontally projected area. Subsurface flow is analyzed along the lower segment of the hillslope, varying in elevation from 2760 to 2787 m over a distance of 137 m

(Figure 1b). The lower hillslope surface consists of about 1.0 m thick loam to silt loam soils, overlying about a 2.6 m thick zone of weathering shale, overlying fractured Mancos Shale bedrock. Measurements were obtained at three lower hillslope monitoring stations (PLM1, PLM2, and PLM3/6 depicted in Figure 1c), locations having the advantage of integrating flow and transport from a larger upslope area while groundwater remains within a few meters of the soil surface.

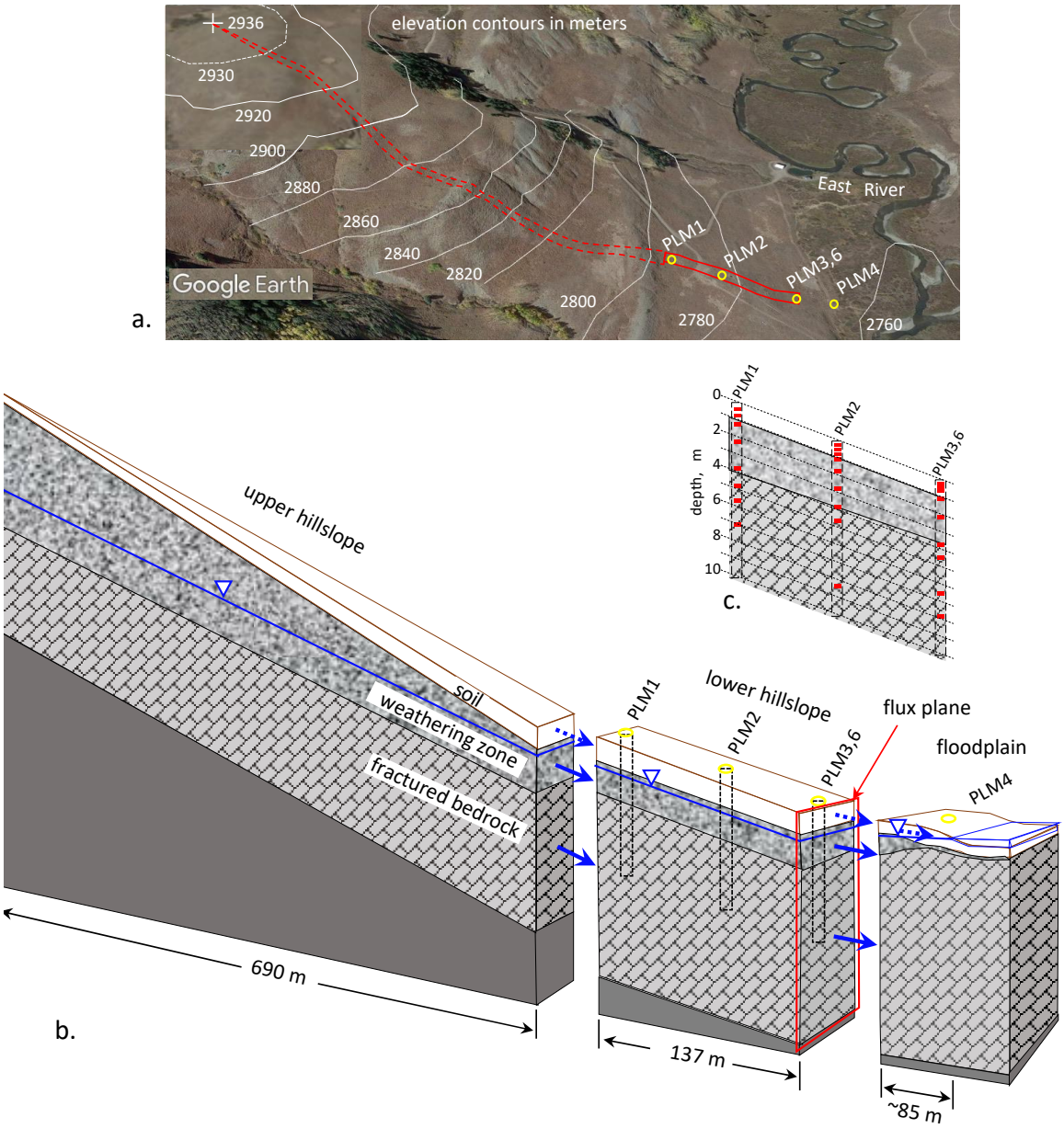

Figure 1. Hillslope site. (**a.**) Aerial view of site and its relation to the East River. (**b.**) Cross-section depiction of upper and lower hillslope sections draining into floodplain and river. The subsurface is subdivided into soil, weathering zone, and fractured bedrock, underlain by

effectively impermeable rock at unknown depth. (**c.)** Cross-section through hillslope boreholes showing depths of sensors and pore water samplers in red.

2.2. Weather data, evapotranspiration, and annual water balance

Daily air temperature and precipitation data were obtained from the Butte SNOTEL weather station (USDA, 2021), located 3.1 km south of the hillslope. This station is 2.2 km closer to the hillslope than the one at Gothic used in our earlier work, and received on average 26% less annual precipitation over WY2017–WY2020. Correlations between Butte SNOTEL air temperatures and shorter-term air temperature data from station ER-CSMWS (Versteeg & Williams, 2021) located 0.3 km from the hillslope were used to estimate daily average (Figure 2a), minimum, and maximum air temperatures at the hillslope needed for *ET* calculations. Because precipitation data at ER-CSMWS are incomplete, the Butte SNOTEL station was used for daily *P* values (Figure 2b) and for calculating daily *ET* for the hillslope (Figure 2c) with the Community Land Model (CLM) (Oleson et al., 2013; Tran et al., 2019). The subsurface hillslope water balance at this site was calculated based on water year cycles that begin on October 1 of the previous calendar year and end on September 30. Although subsurface water storage continues to decrease with the gradually declining water table into March, the selection of October 1 has the advantage of initiating each year without the presence of a snowpack.

An important aspect of the water balance on this hillslope is that although the water table can rise from the weathering zone into the soil during snowmelt, overland flow has never been detected in more than four years of field observations. We also found that summer *ET* is high enough to prevent groundwater recharge by rainfall (T. K. Tokunaga et al., 2019). Therefore, annual subsurface flow is approximated as being equal to annual *P–ET*, as summarized in the table embedded in Figure 2c. Note that annual *P* varied by nearly a factor of 2 between WY2017 with its above-average snowpack and the following snow drought WY2018, and that a similar large difference occurred in WY2019 and WY2020. In contrast, the calculated annual *ET* was less variable from year to year, consistent with findings from other studies (Fatichi & Ivanov, 2014; Garbrecht et al., 2004; Huntington & Billmire, 2014). Given relatively low variability in annual *ET*, magnitudes of annual subsurface flow are expected to be strongly correlated to annual *P*.

Lack of evidence for overland flow (surface runoff, event water) also has important implications for relations between solute concentrations *C* and rates of subsurface discharge *Q* from the hillslope. Models of *C*-*Q* relations for river waters sometime assume that overland flow occurs, and that the dilute endmember water quality is equivalent to that of the precipitation (snow or rainfall) deposited on the watershed (Chanat et al., 2002; Evans & Davies, 1998). More general two-component *C*-*Q* models implicitly include infiltrated rainfall and snowmelt fluxes through the shallow surface as part of the runoff end-member (Miller et al., 2014; Pinder & Jones, 1969). Here, field observations, pore water samples, and the transmissivity feedback analyses indicate that the most dilute endmember in subsurface *C*-*Q* for our hillslope solely consists of snowmelt flowing downslope within the soil while the water table is at its highest level.

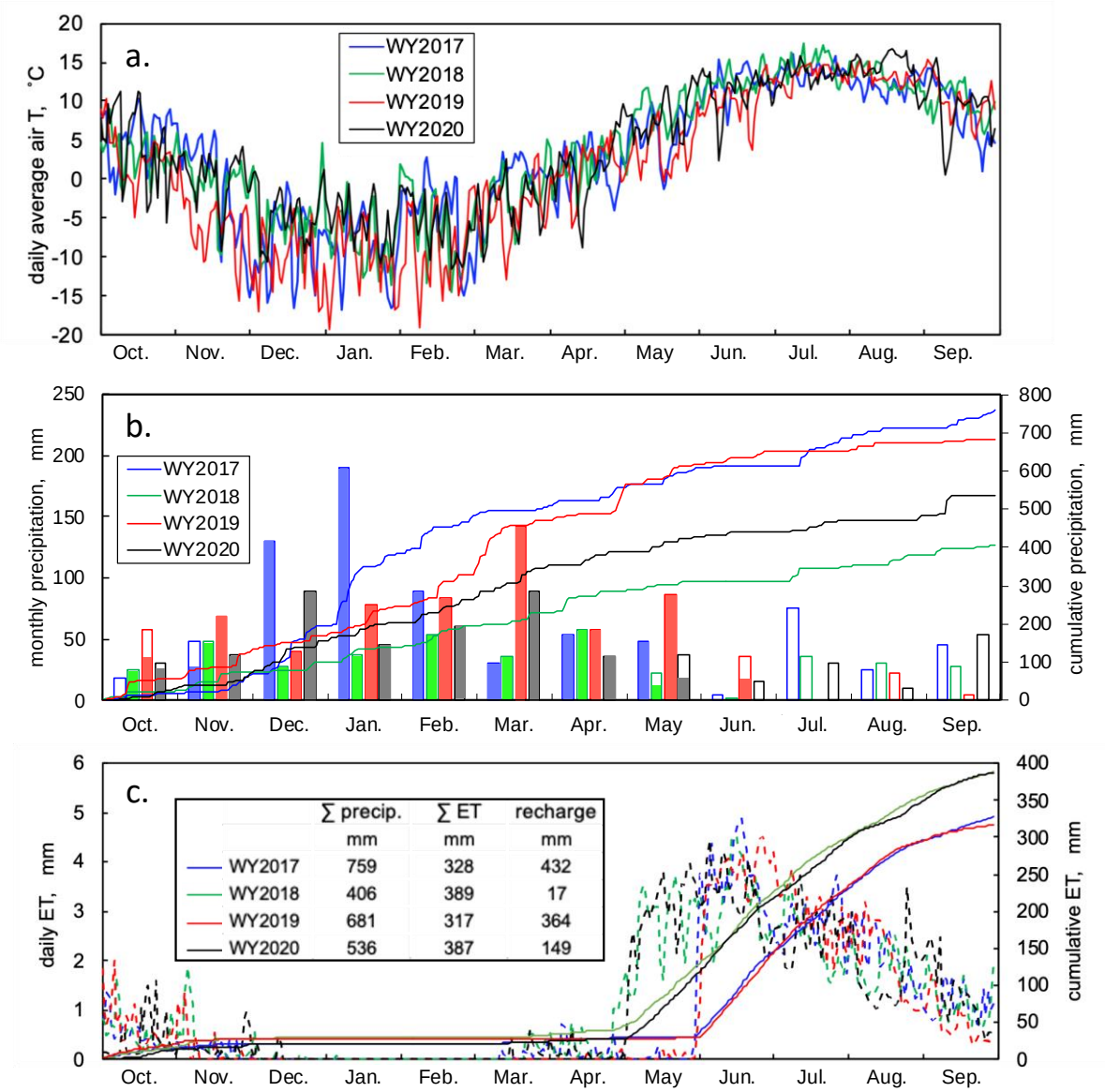

Figure 2. Meteorological conditions at the hillslope site for WY2017–WY2020. (**a.)** Average daily air temperatures. (**b.)** Monthly precipitation (filled bars = snow, unfilled bars = rain). (**c.)** Evapotranspiration calculated with the Community Land Model.

2.3. Hydraulic gradients and transmissivities driving downslope flow

As noted previously, the water table only rises from the weathering zone into the soil during recharge by infiltrating snowmelt, and trends for four years are shown in Figure 3. Differences between of the continuously recorded water table elevations at PLM1 and PLM6 were divided by their separation distance (137 m) to obtain daily values of the hydraulic gradient driving downslope flow. The piezometric gradient along the transect remains similar to the overall slope of the soil surface (0.197 m m^{-1}), and ranges between 0.19 and 0.21 m m^{-1}. Because flows are approximated as occurring parallel to the hillslope's soil surface, with a lower impermeable boundary also assumed to be oriented parallel to the surface, Childs' corrections to the Dupuit-Forchheimer approximation for flow along a sloping water table is now implemented (Childs,

1971). This correction accounts for the unit normal area for groundwater flow being perpendicular to the slope, rather than being vertically oriented. Thus, cross-sectional areas for flow are now obtained by scaling down the saturated vertical thickness by $cos\theta$, where θ is the slope between PLM1 and PLM3. For this hillslope with θ = 11.2˚, $cos\theta$ = 0.98, a minor reduction. However, on steeper hillslopes, this correction becomes important.

In order to calculate downslope flow, the daily average water table elevation along the hillslope is first used to determine the saturated thickness within the weathering zone (1.00–3.60 m depth, *wz*) and within the two soil regions (surface 0–0.50 m depth designated *s1*, deeper 0.50–1.00 m depth designated *s2*). These $cos\theta$ -scaled thicknesses were multiplied by the saturated K assigned to each layer to obtain their respective transmissivities, T_{s1}, T_{s2}, and T_{wz}. It should be noted that downslope flow along the soil is only effective when the water table resides within the soil, hence T_s is usually zero. Because boreholes were drilled to depths of only 10.0 m below ground surface (bgs), deeper flow cannot be quantified. Therefore, the transmissivity of the permanently saturated fractured bedrock T_{fbr} was among the parameters adjusted to match the estimated annual subsurface flux. Daily subsurface flow was equated to the sum of the four T values times the hydraulic gradient, and these daily flows were summed in order to obtain yearly subsurface flow. In our updated approach, K_{s1}, K_{s2}, K_{wz}, and T_{fbr} are adjusted with the objective of minimizing deviations between calculated subsurface fluxes and their respective *P-ET* for WY2017 through WY2020.

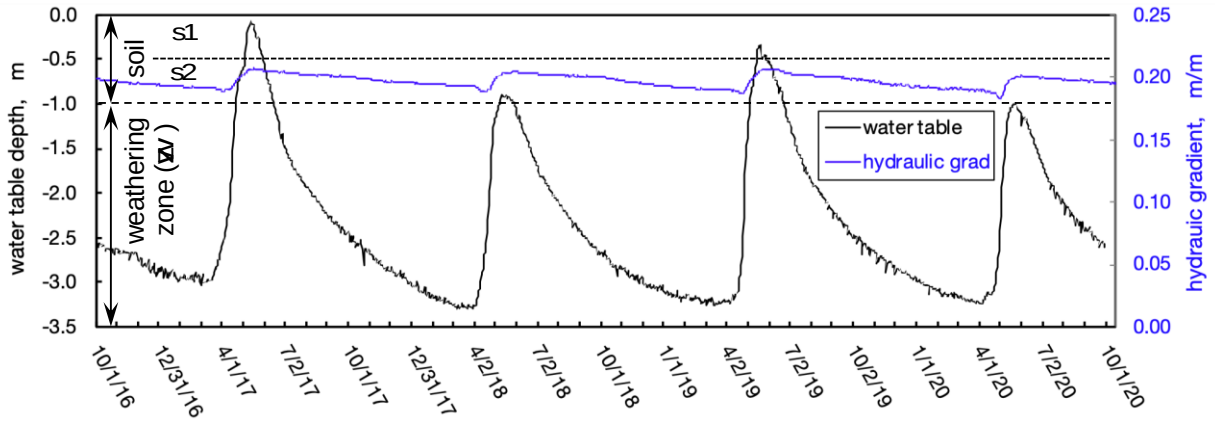

Figure 3. Average water table depth below the soil surface and average hydraulic gradient between PLM1 and PLM3/6. Recharge from melting of the snowpack can raise the water table from the weathering zone into the soil zones *s2* and *s1*.

2.4. Calculating hillslope scale hydraulic properties

To provide a baseline set of subsurface flow predictions for later comparisons, fluxes were initially calculated with representative field-measured K_{s1} = of 7.9 × 10^{-6}, K_{s2} = 9.7 × 10^{-6}, and K_{wz} = 1.1 × 10^{-5} m s^{-1}, as before (T. K. Tokunaga et al., 2019). Because precipitation data from the nearby Butte SNOTEL is now used, *P-ET* = 432 mm for WY2017 (Figure 2c), instead of 562 mm previously obtained based on data from the Gothic weather station (5.3 km up the East River from the hillslope). It is worth noting that average annual P for WY2017–WY2020 at the Butte SNOTEL is only 74% that reported at the more distant Gothic station, leading to generally lower calculated recharge and subsurface flow. Using the measured K_{fbr} = 1.6 × 10^{-7} m s^{-1} requiring a fractured bedrock thickness (b_{fbr}) of 109.9 m in order for the total WY2017 subsurface flow to be

equivalent to 432 mm. This b_{fbr} combined with K_{fbr} is equivalent to T_{fbr} = 1.7 × 10^{-5} m^2 s^{-1}. While this combination of parameters satisfies water mass balance for WY2017, it overestimated recharge (*P-ET*) by 375, 36, and 231 mm for WY2018, WY2019, and WY2020, respectively. For the four water years, the root-mean-square deviation (rmsd) between *P-ET* and subsurface flow was 219 mm, a difference amounting to 37% of the average annual *P*.

The overestimates of subsurface flow, especially during the WY2018 and WY2020 droughts, indicate that flow within the more continuously saturated deeper strata was unrealistically large. Given that the hydraulic gradient remains nearly equal to 0.20 (Figure 3), reductions in K_{wz} and T_{fbr} were indicated. Reduction of the relatively steady deeper subsurface flow in combination with enhancement of snowmelt-dependent shallower downslope flow can improve overall agreement between calculated annual subsurface flow and associated *P-ET*. Amplification of the values assigned to K_{s1} and K_{s2} is indeed warranted based on the previously cited field studies that showed that small scale measurements substantially underestimate *K* at the hillslope scale.

Based on these considerations, all *K* values were varied while keeping b_{fbr} at its original value 109.9 m. The latter constraint actually amounts to using variations in K_{fbr} to represent variations in T_{fbr}. Additional constraints included were that $K_s > K_{wz} > K_{fbr}$, in keeping with original framework of the transmissivity feedback model. It should be noted that K_{s1} was not required to be greater than K_{s2} because studies of soil pipes have provided evidence for hydraulically important buried channels within soils (Uchida et al., 2005). Daily water table-dependent transmissivity-based fluxes for all layers were summed on a yearly basis for WY2017 through WY2020, with variables K_{s1}, K_{s2}, K_{wz}, and T_{fbr} optimized using the Solver regression tool in Microsoft Excel, in order to minimize the root mean-square differences between calculated annual subsurface fluxes and their associated *P-ET*. This procedure was implemented using different initial values for the variables in order to assess suitability of their optimized values.

2.5. Solutes in pore water

Our previous estimate of subsurface weathering rates (Wan et al., 2019) and total dissolve nitrogen (TDN) export rates (Wan et al., 2021) were updated through combining the calibrated hydraulic properties with measurements of base cations (BC) and TDN over the same four water years. As before, base cations (Na^+, K^+, Mg^{2+}, and Ca^{2+}) were analyzed by inductively coupled mass spectrometry, and the sum of base cations ∑BC was expressed in terms of moles of cation charge. A Shimadzu TOC-VCPH equipped with a total nitrogen module was used for determining TDN.

3 Results and Discussion

3.1. Optimized hillslope scale hydraulic properties and subsurface fluxes

Recall that a large average discrepancy of 219 mm per year was obtained for four years (WY2017-WY2020) when measured *K* values were combined with a bedrock thickness adjusted such that total subsurface flow equaled *P-ET* for WY2017. By optimizing *K* to minimized deviations for *P-ET* for both the high snowpack WY2017 and low snowpack WY2018, the four-year rmsd was reduced to 77 mm. Fitting to all four years resulted in optimized values of K_{s1}, K_{s2}, and K_{wz} are 1.4 × 10^{-5}, 4.5 × 10^{-4}, and 2.1 × 10^{-6} m s^{-1}, and the optimized T_{fbr} = 3.4 × 10^{-6} m^2 s^{-1}. This combination of optimized hydraulic properties further reduced the rmsd for subsurface flow versus *P-ET* to 56 mm (9% of the average annual *P*), and predicts very high flow rates along the soil and weathering zones during periods of snowmelt.

The strong temporal dependence of subsurface flow on water table depth is shown in Figure 4. Figure 4a shows the snowmelt-dependent variation in water table depth (left ordinate), and predicted subsurface fluxes transmitted via different zones (logarithmic right ordinate). In this figure, subsurface flow through the transect is expressed in terms of daily volumetric water flow per unit width (normal to the flow direction). Baseflow through the bedrock stays practically steady because it remains fully saturated and the hydraulic gradient only exhibits minor fluctuations during snowmelt events. Flow along the weathering zone fluctuates in response to the continuously varying water table depth that drives continuous variations in T_{wz}. Downslope flow along the soil zones is only activated when snowmelt is sufficient to raise the water table from the weathering zone to within 1.0 m of the hillslope surface, and Figure 3 showed that this occurred each year of this study except for the snow drought WY2020. Although such periods with high water table elevations are short, they facilitate very high flow rates because of the high K_{s1} and K_{s2}. The importance of transmissive flow along the soil during snowmelt is further illustrated in Figure 4b, where subsurface flow in each zone is expressed as a fraction of the daily total subsurface flow. In high snowpack years, over 90% of the snowmelt pulse is transported along the soil while the water table resides within it. Outside of periods dominated by snowmelt, Figure 4b shows that the weathering zone and fractured bedrock annually alternate with respect to their fractional contributions to subsurface flow.

The recharge-dependent patterns shown in Figure 4 point to anticipated changes in subsurface flow and transport resulting from increased frequency of snow drought years. Recall that WY2018 and WY2020 received below-average snowfall, but were preceded by years with above-average snow (Figure 2b). As the frequency of snow droughts increases, depletion of subsurface water storage from back-to-back snow drought years become more common (Alvarez-Garreton et al., 2021). Because such depletion is strongly linked to greater depths of annual water table recession prior to snowmelt recharge, previously continuously water saturated bedrock will become exposed to atmospheric oxygen with greater frequency. Given the importance of water table elevation on oxidative weathering of shale bedrock (Brantley et al., 2013; Wan et al., 2019; Winnick et al., 2017), climate change-induced alteration of the snowpack in mountainous watersheds can be expected to accelerate bedrock weathering.

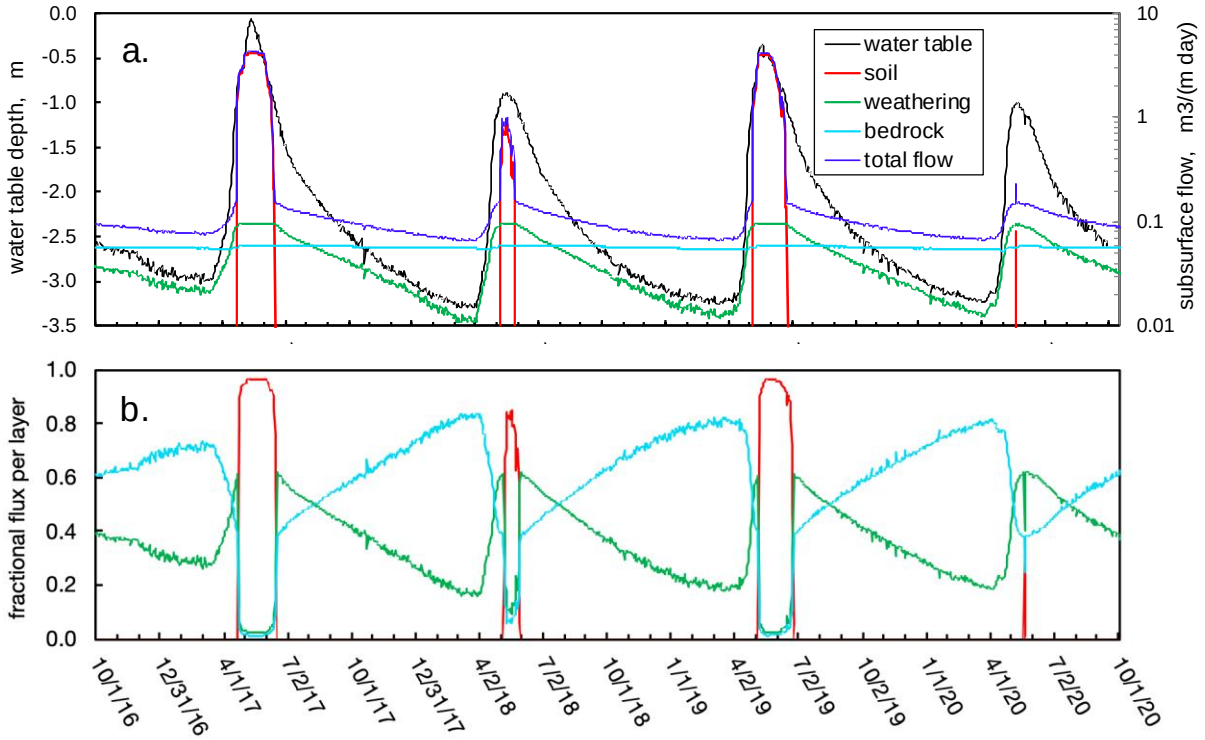

Figure 4. Impacts of water table fluctuations on subsurface flow. (**a.**) Annual variations in water table depth and resulting calculated downslope flow along different zones of the hillslope. (**b.**) Time-dependence of fractional contributions of flow along the soil, weathering zone, and fractured bedrock to overall subsurface flow.

3.2. Transport of solutes

Subsurface flow provides the linkage between the chemistry of hillslope pore waters and solutes delivered to the floodplain and river, specifically as the product of subsurface fluxes and solute concentrations within the different strata. In the following subsections, we present transport calculations for base cations and total dissolved nitrogen, based on their measured pore water concentrations, the Butte SNOTEL weather data, and hydraulic properties optimized for subsurface flow matching *P-ET* over the four water years.

3.2.1. Base cation transport

Previously obtained trends in porewater ∑BC (Wan et al., 2019) were updated through WY2020. In Figure 5a, time trends of individual ∑BC values (smaller, unfilled symbols) are shown along with averages (larger, filled symbols). As in our previous studies, dates associated with pore water samples were interpolated between the sampling date and the previous sampling date in recognition of the time-dependent inflow of pore waters (T. Tokunaga, 1992). Daily ∑BC values between those associated with actual samples were estimated by linear interpolation between measured average values within each zone, and are shown as the line segments in Figure 5a. Although values of ∑BC vary widely, they are distinctly higher in the weathering zone relative to the fractured bedrock and soil, consistent with shale weathering being the primary source of solute release (Wan et al., 2019). Low ∑BC values in soil reflect the diluting influences of recharge from snowmelt. It is important to note that in years with low snowfall, BC concentrations in pore waters discharged during snowmelt are higher not only because of less

water, but also because a larger fraction of flow occurs via the weathering zone (Figure 4b) where dissolution is most active.

Rates of ∑BC export were obtained through multiplying the daily average ∑BC values within each layer by their associated daily flow rates (Figure 4), and presented in Figure 5b. The time trends for ∑BC export reflect the importance of annual snowmelt events that flush hillslope solutes to the floodplain and river. Figure 5b shows that downslope flow via the soil is the dominant pathway for ∑BC export during snowmelt events of 2017-2019. When snowmelt is sufficient to drive the water table up into the soil, the transmissivity of the saturated soil becomes so large that this shallow zone exports most of the base cations despite having low BC concentrations (Figure 5a). In contrast, water table rise did not extend into the soil during WY2020 because of insufficient snowpack and snowmelt, and therefore prevented downslope groundwater flow via the soil.

While flow and transport results shown in Figures 4 and 5 are presented per meter width of the transect, annual BC export rates per unit area of the transect are tabulated within Figure 5b to facilitate comparisons with other watersheds. These latter values result from dividing the annual sum of daily values by the transect area (0.00482 ha). The strong dependence of ∑BC export rates on snowmelt-dependent subsurface flow is evident over the four different water years, being maximum (17.7 $kmol_c\ ha^{-1}\ y^{-1}$) in the highest snowpack WY2017 and minimum (7.1 $kmol_c\ ha^{-1}\ y^{-1}$) in the lowest snowpack WY2020. These ∑BC export rates averaged over four years amount to 12.3 $kmol_c\ ha^{-1}\ y^{-1}$, substantially lower than the previously estimated 55 $kmol_c\ ha^{-1}\ y^{-1}$ average over three years based on calibration of *P-ET* using the more distant weather station data (Wan et al., 2021). These new, lower ∑BC export rates reflect both lower annual recharge (*P-ET* based on the Butte SNOTEL) and higher flow-weighting of dilute soil water during snowmelt resulting from improved estimates of hydraulic properties. These improved ∑BC export rates are well within the broad range (3 to 66 $kmol_c\ ha^{-1}\ y^{-1}$) reported from rivers draining sedimentary bedrock watersheds (Horton et al., 1999; Morrison et al., 2012; Tuttle et al., 2014). A revised lower rate of rock-N release amounting to 4.2 kg N $ha^{-1}\ y^{-1}$ was obtained by multiplying the updated ∑BC by 0.0244 mol $molc^{-1}$, the ratio of N to base cations in Mancos Shale (Wan et al., 2021). This rock-N release is higher than the reactive-N input from atmospheric deposition (2.78 kg N $ha^{-1}\ y^{-1}$ measured in Gothic (CASTNET, 2019)). Assuming that biological N-fixation contributes reactive-N at a similar rate as atmospheric deposition (Darrouzet-Nardi et al., 2012; Wan et al., 2021), the total reactive-N supply rate for the hillslope amounts to 9.8 kg $ha^{-1}\ y^{-1}$, with rock-N supplying the largest input of 43%.

Subsurface *C-Q* relations for base cations were generated by plotting correlations between daily values of flow-weighted ∑BC concentrations (black curve in Figure 5a) and their corresponding total subsurface flow (black dashed curve in Figure 5b), and presented for each water year in Figure 5c. These results are analogous to more familiar *C-Q* relations obtained from measurements in rivers (Chanat et al., 2002; Evans & Davies, 1998; Godsey et al., 2009), but reflect predictions of exports along the hillslope transect rather than integrated responses over broader catchments and watersheds. Characteristics of surface water *C-Q* such as being hysteretic or nonhysteretic, and fitting to the power-law $C = aQ^b$ to describe relations reflecting displacement ($b > 0.1$), chemostasis ($-0.1 \leq b \leq 0.1$), or dilution ($-1 \leq b < -0.1$), are also useful for examining subsurface *C-Q* behavior. From Figure 5c, the annual subsurface *C-Q* for ∑BC is nearly nonhysteretic, with distinctly declining regions describable with $b \sim -0.5$, indicative of dilution behavior expected from annual snowmelt pulses. For comparison, *C-Q* relations for cations in many watershed are nearly chemostatic (Godsey et al., 2009), while in the upper East

River watershed (Winnick et al., 2017) and the nearby Coal Creek (Zhi et al., 2019) weak dilution with b ~ -0.2 have been reported. The strong dilution behavior calculated for the subsurface of this hillslope site is consistent with annual inputs of very low salinity snowmelt pulses superimposed over deeper pore waters enriched through weathering of solute-rich Mancos Shale (Morrison et al., 2012; Tuttle et al., 2014; Wan et al., 2019).

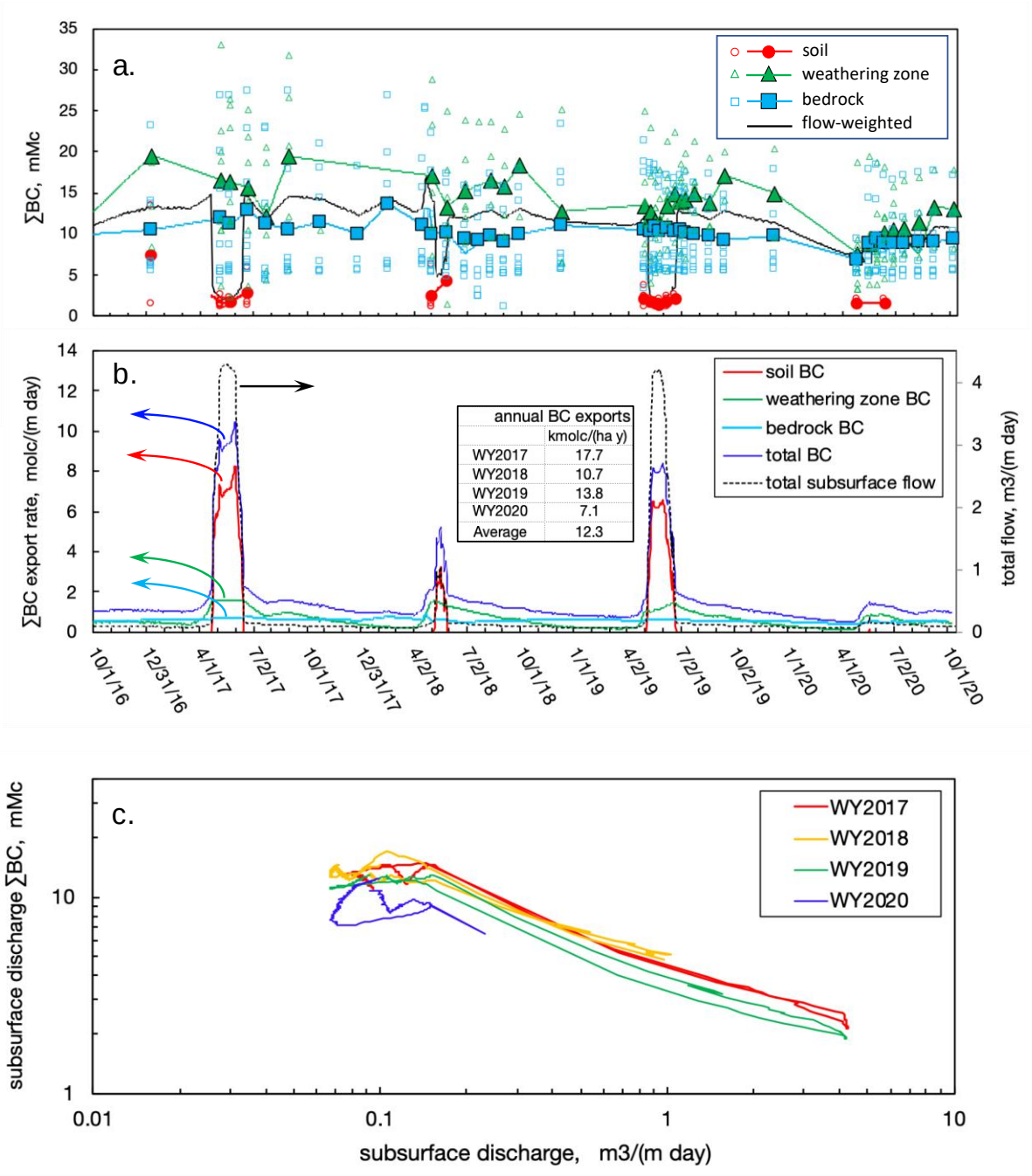

Figure 5. Annual variations in (**a.**) pore water base cation (BC) concentrations, (**b.**) calculated base cation export rates along different zones of the hillslope, and (**c.**) subsurface *C-Q* relation

for base cations, showing that discharge-dependence of annual cycles of flow-weighted ∑BC concentrations reflects dilution from snowmelt.

3.2.2. Transport of dissolved nitrogen

Individual data points for total dissolved nitrogen (TDN) concentration in pore waters from soil, weathering zone, and bedrock, and trendlines through linearly interpolated daily average concentrations in each zone are presented in Figure 6a. These interpolated daily average concentrations were normalized by their associated subsurface fluxes (Figure 4) to obtain overall flow-weighted subsurface TDN concentrations also shown in the figure. Subsurface TDN export rates (Figure 6b), and subsurface *C*-*Q* relations for TDN (Figure 6c) were calculated based on the approach described previously for ∑BC exports. Similar to patterns for ∑BC, highest TDN concentrations occur in the weathering zone, reflecting the dominance of N released by weathering relative to surface inputs from deposition and N-fixation (Wan et al., 2021). Unlike patterns for ∑BC, lowest TDN concentrations occur in the bedrock porewaters, consistent with denitrification in reducing waters. The low redox conditions driving denitrification in the permanently saturated fractured bedrock are also responsible for keeping dissolved uranium concentrations low (Wan et al., 2019). Because the highest rates of downslope fluxes occur when the hillslope becomes most water-saturated, punctuated TDN transport occurs annually during snowmelt, especially when the water table rises into significant fractions of the soil (Figure 6b). Based on the improved estimates of subsurface fluxes, the overall TDN export rate amounts to 3.8 kg N ha^{-1} y^{-1}, a value that is lower than that previously reported (10.6 kg N ha^{-1} y^{-1}) because of both lower overall recharge (based on the Butte SNOTEL data) and greater influence of dilute fluxes via the soil zone during snowmelt. This TDN export rate amounts to 39% of the updated hillslope reactive-N supply rate (9.8 kg N ha^{-1} y^{-1}), indicating that about 61% of the hillslope reactive N is lost to denitrification.

The subsurface *C*-*Q* relation for TDN (Figure 6c) are approximately chemostatic during low snowmelt years (2018, 2019), and exhibit weaker dilution trends relative to base cations for the higher snowmelt years (2017, 2019). The asymmetry in the peaks for total subsurface TDN export rate relative to the peaks in total subsurface flow (Figure 6b) is reflected in clockwise *C*-*Q* hysteresis during major snowmelt events (Figure 6c). These patterns are consistent with TDN depletion over the course of subsurface flow during spring snowmelt. Nitrate accounts for most of the TDN in the hillslope subsurface (Wan et al., 2021), and the hysteretic patterns reflecting dissolved N losses may be attributed to denitrification and assimilation (Burns et al., 2019; Ebeling et al., 2021; Ocampo et al., 2006).

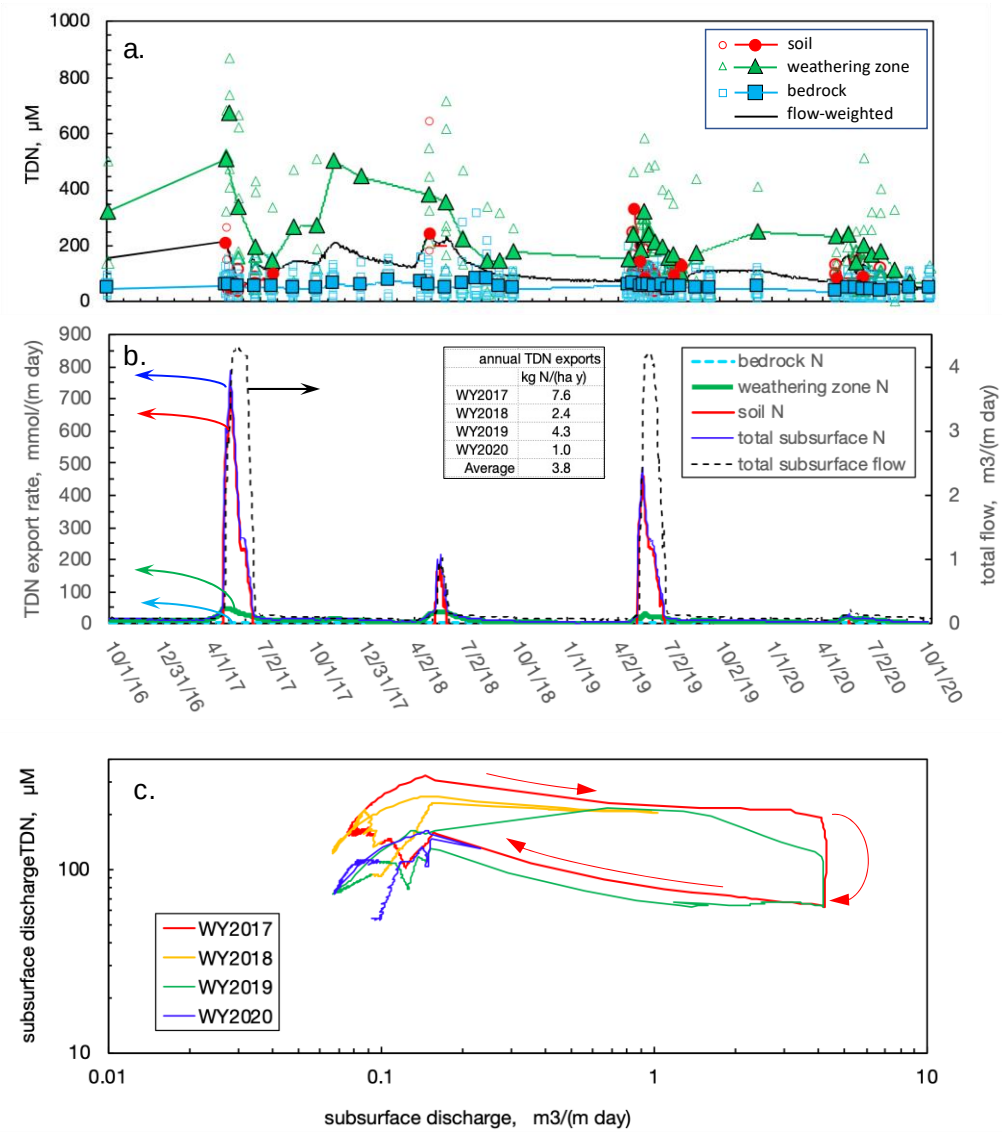

Figure 6. Annual variations in (**a.**) pore water total dissolved nitrogen (TDN) concentrations, (**b.**) calculated TDN export rates along different zones of the hillslope, and (**c.**) subsurface *C*-*Q* relations for TDN over four water years.

4 Conclusions

To better understand subsurface flow and transport in hillslopes receiving precipitation primarily as snow, *P*-*ET* was used to provide water mass balance constraints on annual discharge predicted by the transmissivity feedback model. When constrained by water mass balance over only a single year, transmissivity feedback calculations of snowmelt-driven hillslope flow have large uncertainties because the same total discharge can be obtained with multiple combinations of widely ranging values of *K* assigned to the different subsurface zones (T. K. Tokunaga et al., 2019). Because the highly permeable soil only directly contributes to downslope transmissivity flow during years with higher recharge from snowmelt, calibration over both years with above-

and below-average snowpack constrains the hillslope *K* profile to its optimal values. Thus, improvements to the transmissivity feedback model of subsurface flow at the hillslope were obtained by optimizing *K* values such that predicted discharges best matched *P-ET* for four years having large differences in *P-ET*. The optimized *K* values of the soil layers are one to two orders of magnitude greater than that of the underlying weathering shale, and facilitate rapid discharge of snowmelt via temporarily shallow groundwater flow. The resulting hydrograph for subsurface flow during snowmelt rises and falls rapidly, resembling hydrographs of flashy runoff in rivers.

Despite the fact that solute concentrations in soil pore waters are generally low, hillslope solute exports during snowmelt in most years largely occur via the soil because of very rapid shallow groundwater flow within the highly transmissive saturated soil. Updated pore water data presented here further support our recent findings that bedrock weathering is the primary source for base cations and reactive nitrogen discharged from the hillslope (Wan et al., 2021; Wan et al., 2019). Acceleration of bedrock weathering from consecutive snow drought years is anticipated to result from water table lowering to greater depths, exposing previously permanently reducing shale bedrock to oxygen and driving dissolution of pyrite and carbonate minerals.

Following calibration of the transmissivity profile with years having widely differing *P-ET*, future subsurface flow and transport can be estimated based only on measurements of water table depth and pore water chemistry. The ability to represent flow and transport over wide ranges of input from snowmelt is attractive in view of large interannual variations in annual snowfall and anticipated climate change-driven increased frequency of snow drought years (Dierauer et al., 2019; Marshall et al., 2019; Shrestha et al., 2021). Given its simplicity, this approach can be used for estimating subsurface flow and transport in many other catchments recharged primarily through snowmelt.

Acknowledgments

This work was conducted as part of the Watershed Function Scientific Focus Area at Lawrence Berkeley National Laboratory and was supported by the U.S. Department of Energy (DOE) Subsurface Biogeochemical Research Program, DOE Office of Science, Office of Biological and Environmental Research, under Contract Number DE-AC02-05CH11231.

Data Availability

Data used in this paper to be deposited in the U.S. DOE Environmental Systems Science Data Infrastructure for a Virtual Ecosystem (ESS-DIVE).

References

Alvarez-Garreton, C., Boisier, J. P., Garreaud, R., Seibert, J., & Vis, M. (2021). Progressive water deficits during multiyear droughts in basins with long hydrological memory in Chile. *Hydrology and Earth System Sciences, 25*(1), 429-446. <Go to ISI>://WOS:000614265600001

Ameli, A. A., Beven, K., Erlandsson, M., Creed, I. F., McDonnell, J. J., & Bishop, K. (2017). Primary weathering rates, water transit times, and concentration-discharge relations: A theoretical analysis for the critical zone. *Water Resources Research, 53*(1), 942-960. <Go to ISI>://WOS:000394911200055

Anderson, S. P., & Dietrich, W. E. (2001). Chemical weathering and runoff chemistry in a steep headwater catchment. *Hydrological Processes, 15*(10), 1791-1815. <Go to ISI>://WOS:000169965300009

Arnone, E., Noto, L. V., Lepore, C., & Bras, R. L. (2011). Physically-based and distributed approach to analyze rainfall-triggered landslides at watershed scale. *Geomorphology, 133*(3-4), 121-131. <Go to ISI>://WOS:000295544400002

Bishop, K., Seibert, J., Koher, S., & Laudon, H. (2004). Resolving the double paradox of rapidly mobilized old water with highly variable responses in runoff chemistry. *Hydrological Processes, 18*(1), 185-189. <Go to ISI>://WOS:000188506700013

Boggs, J. M., & Adams, E. E. (1992). Field-study of dispersion in a heterogeneous aquifer. 4. Investigation of adsorption and sampling bias. *Water Resources Research, 28*(12), 3325-3336. <Go to ISI>://WOS:A1992KD06700022

Brantley, S. L., Holleran, M. E., Jin, L. X., & Bazilevskaya, E. (2013). Probing deep weathering in the Shale Hills Critical Zone Observatory, Pennsylvania (USA): the hypothesis of nested chemical reaction fronts in the subsurface. *Earth Surface Processes and Landforms, 38*(11), 1280-1298. <Go to ISI>://WOS:000323733600008

Brooks, E. S., Boll, J., & McDaniel, P. A. (2004). A hillslope-scale experiment to measure lateral saturated hydraulic conductivity. *Water Resources Research, 40*(4). <Go to ISI>://WOS:000221088600004

Burns, D. A., Pellerin, B. A., Miller, M. P., Capel, P. D., Tesoriero, A. J., & Duncan, J. M. (2019). Monitoring the riverine pulse: Applying high-frequency nitrate data to advance integrative understanding of biogeochemical and hydrological processes. *Wiley Interdisciplinary Reviews-Water, 6*(4). <Go to ISI>://WOS:000471709400001

CASTNET. (2019). Clean Air Status and Trends Network (CASTNET). Retrieved October 29, 2019, from United States Environmental Protection Agency https://java.epa.gov/castnet/datatypepage.do?reportTypeLabel=Historical%20Deposition%20Data&reportTypeId=REP_006

Cayan, D. R. (1996). Interannual climate variability and snowpack in the western United States. *Journal of Climate, 9*(5), 928-948. <Go to ISI>://WOS:A1996UN85600003

Chanat, J. G., Rice, K. C., & Hornberger, G. M. (2002). Consistency of patterns in concentration-discharge plots. *Water Resources Research, 38*(8). <Go to ISI>://WOS:000179643600002

Childs, E. C. (1971). Drainage of groundwater resting on a sloping bed. *Water Resources Research, 7*(5), 1256-1263. <Go to ISI>://WOS:A1971K717900021

Darrouzet-Nardi, A., Erbland, J., Bowman, W. D., Savarino, J., & Williams, M. W. (2012). Landscape-level nitrogen import and export in an ecosystem with complex terrain, Colorado Front Range. *Biogeochemistry, 109*(1-3), 271-285. <Go to ISI>://WOS:000303377800019

Di Prima, S., Marrosu, R., Lassabatere, L., Angulo-Jaramillo, R., & Pirastru, M. (2018). In situ characterization of preferential flow by combining plot- and point-scale infiltration experiments on a hillslope. *Journal of Hydrology, 563*, 633-642. <Go to ISI>://WOS:000441492700051

Dierauer, J. R., Allen, D. M., & Whitfield, P. H. (2019). Snow drought risk and susceptibility in the western United States and southwestern Canada. *Water Resources Research, 55*(4), 3076-3091. <Go to ISI>://WOS:000468597900027

Ebeling, P., Kumar, R., Weber, M., Knoll, L., Fleckenstein, J. H., & Musolff, A. (2021). Archetypes and controls of riverine nutrient export across German catchments. *Water Resources Research, 57*(4). <Go to ISI>://WOS:000644063800067

Evans, C., & Davies, T. D. (1998). Causes of concentration/discharge hysteresis and its potential as a tool for analysis of episode hydrochemistry. *Water Resources Research, 34*(1), 129-137. <Go to ISI>://WOS:000071367100013

Fatichi, S., & Ivanov, V. Y. (2014). Interannual variability of evapotranspiration and vegetation productivity. *Water Resources Research, 50*(4), 3275-3294.

Garbrecht, J., Van Liew, M., & Brown, G. O. (2004). Trends in precipitation, streamflow, and evapotranspiration in the Great Plains of the United States. *Journal of Hydrological Engineering, 9*(5), 360-367.

Glaser, B., Jackisch, C., Hopp, L., & Klaus, J. (2019). How meaningful are plot-scale observations and simulations of preferential flow for catchment models? *Vadose Zone Journal, 18*(1), 180146. <Go to ISI>://WOS:000468872600001

Glaser, B., Klaus, J., Frei, S., Frentress, J., Pfister, L., & Hopp, L. (2016). On the value of surface saturated area dynamics mapped with thermal infrared imagery for modeling the hillslope-riparian-stream continuum. *Water Resources Research, 52*(10), 8317-8342. <Go to ISI>://WOS:000388493400044

Godsey, S. E., Kirchner, J. W., & Clow, D. W. (2009). Concentration-discharge relationships reflect chemostatic characteristics of US catchments. *Hydrological Processes, 23*(13), 1844-1864. <Go to ISI>://WOS:000267321400003

Godt, J. W., Baum, R. L., Savage, W. Z., Salciarini, D., Schulz, W. H., & Harp, E. I. (2008). Transient deterministic shallow landslide modeling: Requirements for susceptibility and hazard assessments in a GIS framework. *Engineering Geology, 102*(3-4), 214-226. <Go to ISI>://WOS:000261723800011

Horton, T. W., Chamberlain, C. P., Fantle, M., & Blum, J. D. (1999). Chemical weathering and lithologic controls of water chemistry in a high-elevation river system: Clark's Fork of the Yellowstone River, Wyoming and Montana. *Water Resources Research, 35*(5), 1643-1655. <Go to ISI>://WOS:000079992400027

Huntington, T. G., & Billmire, M. (2014). Trends in precipitation, runoff, and evapotranspiration of rivers draining to the Gulf of Maine in the United States. *Journal of Hydrometeorology, 15*(2), 726-743.

Jencso, K. G., McGlynn, B. L., Gooseff, M. N., Bencala, K. E., & Wondzell, S. M. (2010). Hillslope hydrologic connectivity controls riparian groundwater turnover: Implications of catchment structure for riparian buffering and stream water sources. *Water Resources Research, 46*, W10524. <Go to ISI>://WOS:000283100600002

Kendall, K. A., Shanley, J. B., & McDonnell, J. J. (1999). A hydrometric and geochemical approach to test the transmissivity feedback hypothesis during snowmelt. *Journal of Hydrology, 219*(3-4), 188-205. <Go to ISI>://WOS:000081294600005

Lute, A. C., & Abatzoglou, J. T. (2014). Role of extreme snowfall events in interannual variability of snowfall accumulation in the western United States. *Water Resources Research, 50*(4), 2874-2888. <Go to ISI>://WOS:000336026000007

Marshall, A. M., Abatzoglou, J. T., Link, T. E., & Tennant, C. J. (2019). Projected changes in interannual variability of peak snowpack amount and timing in the western United States. *Geophysical Research Letters, 46*(15), 8882-8892. <Go to ISI>://WOS:000483812500031

McGuire, K. J., & McDonnell, J. J. (2010). Hydrological connectivity of hillslopes and streams: Characteristic time scales and nonlinearities. *Water Resources Research, 46*, W10543. <Go to ISI>://WOS:000283776800001

Miller, M. P., Susong, D. D., Shope, C. L., Heilweil, V. M., & Stolp, B. J. (2014). Continuous estimation of baseflow in snowmelt-dominated streams and rivers in the Upper Colorado River Basin: A chemical hydrograph separation approach. *Water Resources Research, 50*(8), 6986-6999. <Go to ISI>://WOS:000342632300042

Morrison, S. J., Goodknight, C. S., Tigar, A. D., Bush, R. P., & Gil, A. (2012). Naturally Occurring Contamination in the Mancos Shale. *Environmental Science & Technology, 46*(3), 1379-1387. <Go to ISI>://WOS:000299864400015

Ocampo, C. J., Oldham, C. E., Sivapalan, M., & Turner, J. V. (2006). Hydrological versus biogeochemical controls on catchment nitrate export: a test of the flushing mechanism. *Hydrological Processes, 20*(20), 4269-4286. <Go to ISI>://WOS:000243161300002

Oleson, K. W., Lawrence, D. M., Bonan, G. B., Drewniak, B., Huang, M., Koven, C. D., et al. (2013). *Technical description of version 4.5 of the Community Land Model (CLM)*. Retrieved from Boulder, Colorado:

Penna, D., van Meerveld, H. J., Oliviero, O., Zuecco, G., Assendelft, R. S., Dalla Fontana, G., & Borga, M. (2015). Seasonal changes in runoff generation in a small forested mountain catchment. *Hydrological Processes, 29*(8), 2027-2042. <Go to ISI>://WOS:000352564200012

Pinder, G. F., & Jones, J. F. (1969). Determination of the ground-water component of peak discharge from chemistry of total runoff. *Water Resources Research, 5*(2), 438-&. <Go to ISI>://WOS:A1969D030200012

Rodhe, A. (1989). On the generation of stream runoff in till soils. *Nordic Hydrology, 20*(1), 1-8. <Go to ISI>://WOS:A1989U255100001

Shrestha, R. R., Bonsal, B. R., Bonnyman, J. M., Cannon, A. J., & Najafi, M. R. (2021). Heterogeneous snowpack response and snow drought occurrence across river basins of northwestern North America under 1.0˚C to 4.0˚C global warming. *Climatic Change, 164*(3-4). <Go to ISI>://WOS:000619159100001

Spencer, S. A., Anderson, A. E., Silins, U., & Collins, A. L. (2021). Hillslope and groundwater contributions to streamflow in a Rocky Mountain watershed underlain by glacial till and fractured sedimentary bedrock. *Hydrology and Earth System Sciences, 25*(1), 237-255. <Go to ISI>://WOS:000611365400001

Tokunaga, T. (1992). The pressure response of the soil water sampler and possibilities for simultaneous soil solution sampling and tensiometry. *Soil Science, 154*(3), 171-183.

Tokunaga, T. K., Wan, J., Williams, K. H., Brown, W., Henderson, A., Kim, Y., et al. (2019). Depth- and time-resolved distributions of snowmelt-driven hillslope subsurface flow and transport and their contributions to surface waters. *Water Resources Research, 55*, 9474-9499.

Tran, A. P., Rungee, J., Faybishenko, B., Dafflon, B., & Hubbard, S. S. (2019). Assessment of spatiotemporal variability of evapotranspiration and its governing factors in a mountainous watershed. *Water, 11*, 243.

Tuttle, M. L. W., Fahy, J. W., Elliott, J. G., Grauch, R. I., & Stillings, L. L. (2014). Contaminants from Cretaceous black shale: II. Effect of geology, weathering, climate, and land use on salinity and selenium cycling, Mancos Shale landscapes, southwestern United States. *Applied Geochemistry, 46*, 72-84. <Go to ISI>://WOS:000336654900007

Uchida, T., Kosugi, K., & Mizuyama, T. (2001). Effects of pipeflow on hydrological process and its relation to landslide: a review of pipeflow studies in forested headwater catchments. *Hydrological Processes, 15*(11), 2151-2174. <Go to ISI>://WOS:000170611800006

Uchida, T., Meerveld, I. T., & McDonnell, J. J. (2005). The role of lateral pipe flow in hillslope runoff response: an intercomparison of non-linear hillslope response. *Journal of Hydrology, 311*(1-4), 117-133. <Go to ISI>://WOS:000232174600009

USDA, N. (2021). Colorado SNOTEL Site Butte (380). Retrieved from https://wcc.sc.egov.usda.gov/nwcc/site?sitenum=380

Versteeg, R., & Williams, K. H. (2021). LBNL SFA 2.0 Data Management Site. Retrieved from https://lbnlsfa.paf.subsurfaceinsights.com/login/?redir=%2Fdatadownload%2F&show_redir_msg=1

Wan, J. M., Tokunaga, T. K., Brown, W., Newman, A. W., Dong, W. M., Bill, M., et al. (2021). Bedrock weathering contributes to subsurface reactive nitrogen and nitrous oxide emissions. *Nature Geoscience, 14*(4), 217—224. <Go to ISI>://WOS:000636946800001

Wan, J. M., Tokunaga, T. K., Williams, K. H., Dong, W. M., Brown, W., Henderson, A. N., et al. (2019). Predicting sedimentary bedrock subsurface weathering fronts and weathering rates. *Scientific Reports, 9*. <Go to ISI>://WOS:000497712000043

Weihermuller, L., Kasteel, R., & Vereecken, H. (2006). Soil heterogeneity effects on solute breakthrough sampled with suction cups: Numerical simulations. *Vadose Zone Journal, 5*(3), 886-893. <Go to ISI>://WOS:000242178600009

Weiler, M., McDonnell, J. J., Tromp-van Meerveld, I., & Uchida, T. (2005). Subsurface Stormflow. In M. G. Anderson (Ed.), *Encyclopedia of Hydrological Sciences* (Vol. 112, pp. 14). Hoboken, NJ: John Wiley & Sons, Ltd.

Wilson, G. V., Rigby, J. R., Ursic, M., & Dabney, S. M. (2016). Soil pipe flow tracer experiments: 1. Connectivity and transport characteristics. *Hydrological Processes, 30*(8), 1265-1279. <Go to ISI>://WOS:000373959500008

Winnick, M. J., Carroll, R. W. H., Williams, K. H., Maxwell, R. M., Dong, W. M., & Maher, K. (2017). Snowmelt controls on concentration-discharge relationships and the balance of oxidative and acid-base weathering fluxes in an alpine catchment, East River, Colorado. *Water Resources Research, 53*(3), 2507-2523. <Go to ISI>://WOS:000400160500042

Woodhouse, C. A., & Pederson, G. T. (2018). Investigating runoff efficiency in upper Colorado River streamflow over past centuries. *Water Resources Research, 54*(1), 286-300. <Go to ISI>://WOS:000428474000017

Xiao, M., Udall, B., & Lettenmaier, D. P. (2018). On the causes of declining Colorado River streamflows. *Water Resources Research, 54*(9), 6739-6756. <Go to ISI>://WOS:000448088100050

Zhi, W., Li, L., Dong, W. M., Brown, W., Kaye, J., Steefel, C., & Williams, K. H. (2019). Distinct source water chemistry shapes contrasting concentration-discharge patterns. *Water Resources Research, 55*(5), 4233-4251. <Go to ISI>://WOS:000474848500035